NANO LETTERS

pubs.acs.org/NanoLett

Letter

Rh/Al Nanoantenna Photothermal Catalyst for Wide-Spectrum Solar-Driven CO_2 Methanation with Nearly 100% Selectivity

Gao Fu,[‖] Minghang Jiang,[‖] Jie Liu,[‖] Kaiqiang Zhang, Yi Hu, Yan Xiong, Anyang Tao, Zuoxiu Tie, and Zhong Jin*

Cite This: *Nano Lett.* 2021, 21, 8824–8830

Read Online

ACCESS | Metrics & More | Article Recommendations | Supporting Information

ABSTRACT: Solar-powered CO_2 conversion represents a promising green and sustainable approach for achieving a carbon-neutral economy. However, the rational design of a wide-spectrum sunlight-driven catalysis system for effective CO_2 reduction is an ongoing challenge. Herein, we report the preparation of a rhodium/aluminum (Rh/Al) nanoantenna photothermal catalyst that can utilize a broad range of sunlight (from ultraviolet to the near-infrared region) for highly efficient CO_2 methanation, achieving a high CH_4 selectivity of nearly 100% and an unprecedented CH_4 productivity of 550 $mmol \cdot g^{-1} \cdot h^{-1}$ under concentrated simulated solar irradiation (11.3 $W \cdot cm^{-2}$). Detailed control experiment results verified that the CO_2 methanation process was facilitated by the localized surface plasmonic resonance and nanoantenna effects of the Rh/Al nanostructure under light irradiation. In operando temperature-programmed Fourier transform infrared spectroscopy confirmed that CO_2 methanation on the Rh/Al nanoantenna catalyst was a multistep reaction with CO as a key intermediate. The design of a wide-spectrum solar-driven photothermal catalyst provides a feasible strategy for boosting CO_2-to-fuel conversion.

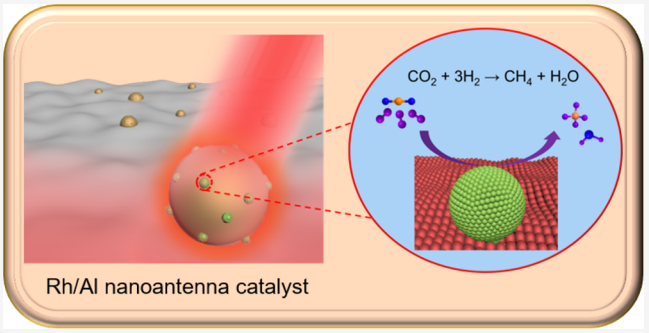

KEYWORDS: *Photothermal CO_2 Methanation, Localized Surface Plasmon Resonance, Nanoantenna Effect, Wide-Spectrum Solar Energy Utilization, High Selectivity*

INTRODUCTION

The hydrogenation of CO_2 to value-added hydrocarbon products by solar power is a promising strategy to establish a carbon-neutral economy.[1−3] However, photocatalytic CO_2 methanation still suffers from poor light absorption,[4,5] a slow reaction rate,[6] and the competitive hydrogen evolution reaction.[7,8] In recent years, transition metal-based localized surface plasmonic resonance (LSPR) photocatalysts have been explored for CO_2 reduction.[9,10] They could utilize ultraviolet or purple light to generate hot electrons, which could be injected into the carbonate intermediate species and drive the stepwise CO_2 methanation reaction.[11] In addition, the transition metal-based LSPR nanostructure could convert the incident light energy into a high surface temperature and strong electric field to activate CO_2 and promote the restructuring of chemical bonds.[12,13] Both the photoelectronic and photothermal processes could drive the CO_2 methanation reaction.[14] However, the resonant frequencies of most transition metals, except for Au and Cu, are in the ultraviolet (UV) or purple light region, which accounts for only approximately 4−7% of the whole solar spectrum,[15] resulting in low solar energy conversion efficiencies. Additionally, assistant heating is normally required to promote the LSPR-based photocatalytic CO_2 methanation reaction.[16] Given the fact that most transition metals cannot simultaneously fulfill all the requirements of light absorption, catalytic activity, and chemical stability,[16−18] it is challenging to design high-performance LSPR photocatalysts with wide-spectrum sunlight absorption and conversion properties for achieving highly efficient solar-driven CO_2 methanation.

Herein, we report the design of a Rh/Al nanoantenna catalyst for wide-spectrum photothermal CO_2 methanation, with an unprecedented CH_4 yield rate and nearly 100% selectivity. In this work, Rh and closely packed Al nanostructures were combined to construct the Rh/Al nanoantenna photocatalyst, where Rh provides abundant active sites for CO_2 methanation and the strong LSPR effect of the Al nanostructure could convert solar energy into hot electrons, generating a high surface temperature and strong localized electric fields to activate the absorbed reactants. A series of wavelength-dependent control experiments proved

Received: August 19, 2021
Revised: October 4, 2021
Published: October 7, 2021

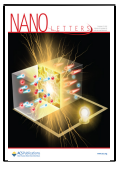

https://doi.org/10.1021/acs.nanolett.1c03215
Nano Lett. 2021, 21, 8824–8830

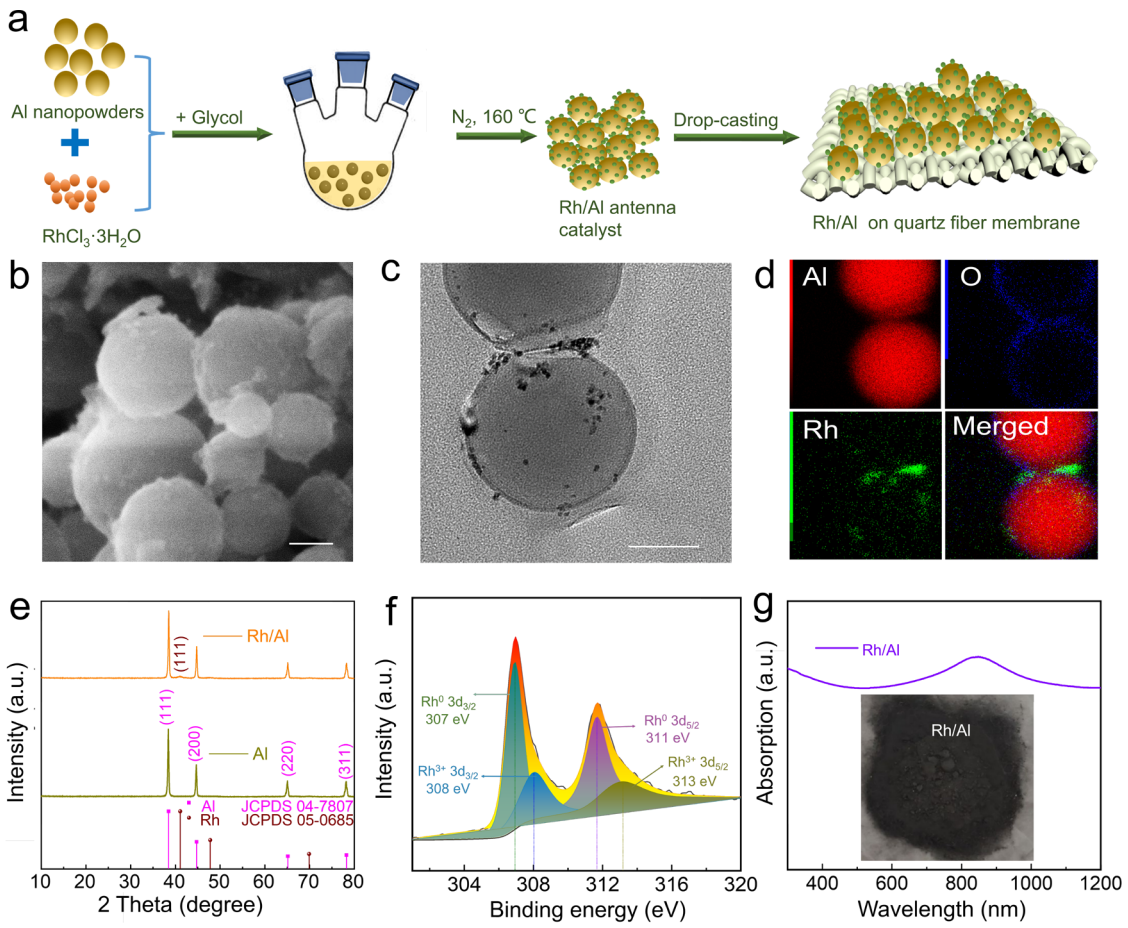

Figure 1. Preparation and characterizations of the Rh/Al nanoantenna photothermal catalyst. (a) Schematic preparation process and (b) SEM, (c) TEM, and (d) corresponding elemental mapping images of the Rh/Al nanoantenna catalyst. (e) XRD patterns of the Rh/Al nanoantenna catalyst and the pristine Al nanopowder. (f) XPS and (g) UV−vis absorption spectra of the Rh/Al nanoantenna catalyst. Scale bars are 50 nm.

that the Al nanostructure could absorb and convert the incident sunlight from the UV region to the NIR region (300−1000 nm) to generate a strong surface temperature field as high as 700 °C, thus effectively promoting photothermal CO_2 reduction and greatly improving CH_4 selectivity and productivity. In addition, we also verified that the photothermal CO_2 methanation driven by the Rh/Al nanoantenna catalyst was a temperature-dependent multistep CO_2 reduction reaction with CO as the key intermediate.

RESULTS AND DISCUSSION

The schematic preparation process of the Rh/Al nanoantenna catalyst is displayed in Figure 1a. Briefly, an Al nanopowder in a spheric morphology with approximately 40−100 nm in diameter (Figure S1) was prepared by the electric explosion of Al wires.[19] Upon the exposure to air, the Al was coated by an 1−2 nm thick amorphous Al_2O_3 layer (Figure S1c).[20] Ultrafine Rh nanoclusters with a 2−3 nm diameter were decorated on the Al nanopowder by the ethylene glycol reduction method using $RhCl_3·3H_2O$ as the Rh precursor, as evidenced by scanning electron microscopy (SEM), transmission electron microscopy (TEM), and corresponding elemental mapping images (Figure 1b−d, respectively). The X-ray diffraction (XRD) pattern of the pristine Al nanopowder exhibits a well-crystallized metal Al phase (JCPDS 04-7807) (Figure 1e). The peaks at 38.5°, 44.7°, 65.1°, and 78.2° correspond to the Al (111), (200), (220), and (311) crystalline planes, respectively. After loading the Rh nanoclusters, the XRD pattern of the Rh/Al nanoantenna catalyst shows a broad peak at 41.0° corresponding to the (111) planes of Rh. The widths and intensities of the Al-related XRD peaks remain almost the same, suggesting that the metal phase of Al is well-preserved. X-ray photoelectron spectroscopy (XPS) analysis (Figure 1f) verified that the Rh nanoclusters loaded on the Rh/Al nanoantenna catalyst possessed a mixed phase of metal Rh and Rh_2O_3,[21] probably due to the surface oxidation of Rh after exposure to air. The UV−vis absorption spectrum of the Rh/Al nanoantenna catalyst (Figure 1g) shows a strong light absorption capability from the UV region to the NIR region, suggesting that its broad-range sunlight absorption properties resulted from the intense LSPR effect of Al.

Photothermal CO_2 methanation tests were performed in a sealed reaction chamber with a sapphire optical window under the concentrated light irradiation of a solar simulator (Figure S2). The schematic photothermal CO_2 methanation process on the Rh/Al nanoantenna catalyst is illustrated in Figure 2a. The actual local surface temperature of the Rh/Al nanoantenna catalyst under different intensities of concentrated simulated sunlight was measured in operando by a FOTRIC 280 infrared camera (Figure S3). Figure 2b summarizes the as-measured surface temperatures of the Rh/Al nanoantenna catalyst under different simulated sunlight intensities. As the light intensity increased from 5.9 to 11.3 $W·cm^{-2}$, the surface temperature increased from 450 °C to approximately 700 °C. Under the

https://doi.org/10.1021/acs.nanolett.1c03215
Nano Lett. 2021, 21, 8824−8830

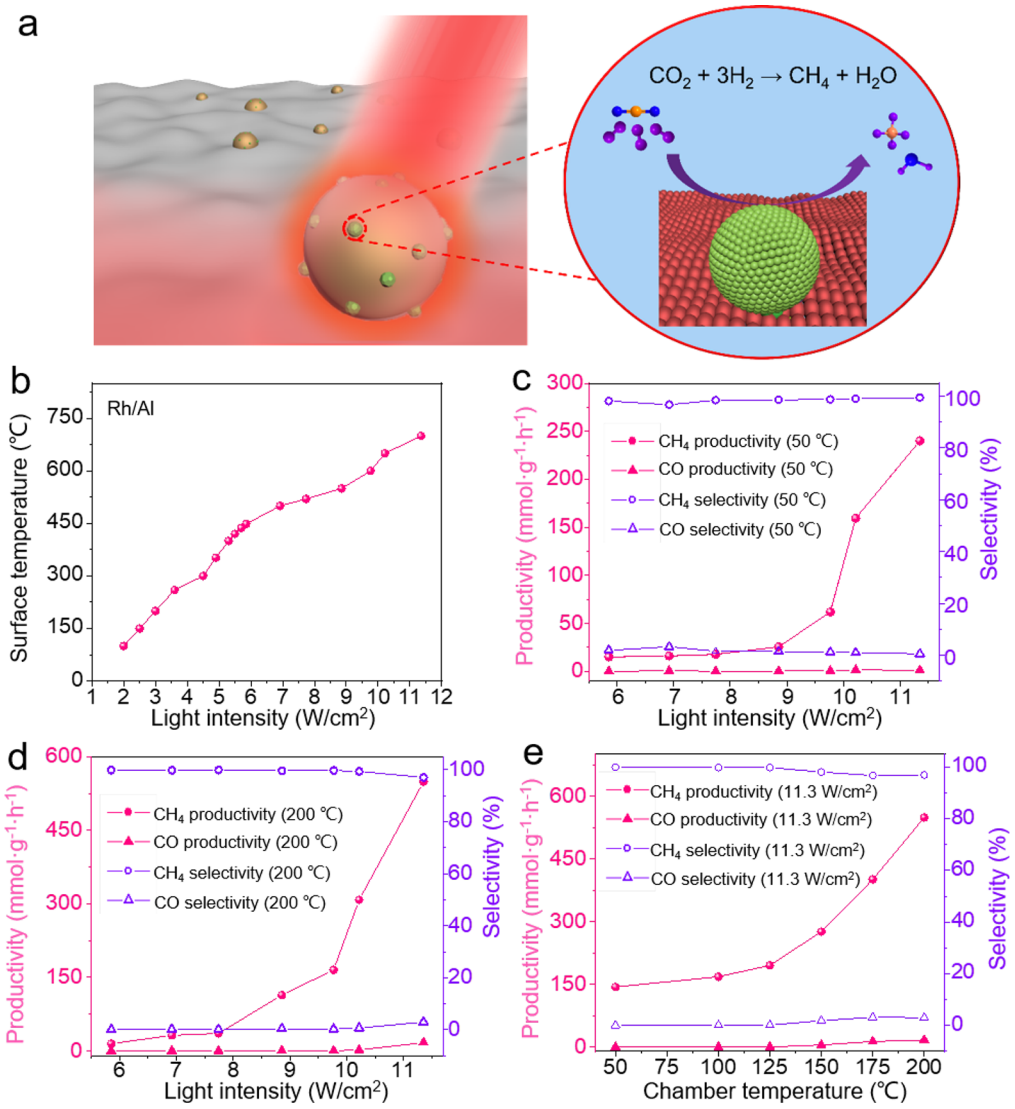

Figure 2. Photothermal CO_2 methanation process of the Rh/Al nanoantenna catalyst under different light intensities and chamber temperatures. (a) Schematic diagrams of photothermal CO_2 methanation on the Rh/Al nanoantenna catalyst. (b) In-operando infrared camera measured surface temperatures of the Rh/Al nanoantenna catalyst under different concentrated simulated sunlight intensities at a chamber temperature of 50 °C. CH_4 and CO productivity and selectivity under different simulated sunlight intensities at the chamber temperatures of (c) 50 and (d) 200 °C. (e) CH_4 and CO productivity and selectivity under concentrated sunlight irradiation of 11.3 W·cm^{-2} at different chamber temperatures.

light intensity of 11.3 W·cm^{-2}, the CH_4 productivity was measured to be 240 mmol·g^{-1}·h^{-1} at a constant chamber temperature of 50 °C (Figure 2c). As the incident light intensity was increased from 5.9 to 7.7 W·cm^{-2}, the CH_4 production rate only slightly increased from 15 to 18 mmol·g^{-1}·h^{-1} (Figure 2c). However, once the light intensity was further increased from 8.9 to 11.3 W·cm^{-2}, the CH_4 production rate sharply increased from 26 to 240 mmol·g^{-1}·h^{-1}. These results suggest that the solar-driven CO_2 methanation of the Rh/Al nanoantenna catalyst was a photothermal reaction rather than a conventional photocatalytic reaction promoted by photogenerated electrons.[12,13] Notably, the CH_4 selectivity under different light intensities was maintained at nearly 100%, with only a tiny amount of CO as gaseous byproduct. The liquid byproduct contained only a negligible amount of ethanol, and no HCOOH or CH_3COOH was detected (Figure S4). Moreover, the optimal mass loading ratio of Rh was determined to be ~5 wt % (Figure S5).

To investigate the influence of assistant heating on the photothermal CO_2 methanation, the chamber temperature was increased to 200 °C (Figure 2d). When the light intensity was increased from 5.9 to 7.7 W·cm^{-2}, the CH_4 production rate gradually increased from 16 to 36 mmol·g^{-1}·h^{-1}; as the light intensity was increased from 8.9 to 11.3 W·cm^{-2}, the CH_4 production rate sharply increased from 110 to 550 mmol·g^{-1}·h^{-1}. Moreover, the CH_4 selectivity at a chamber temperature of 200 °C was well maintained at nearly 100% under different light intensities. The above results further verify that the CH_4 productivity measured at the same chamber temperature is not linearly related with the incident light intensity. There is a "critical light intensity" for promoting CH_4 production. If the incident light intensity is higher than the critical light intensity, the CH_4 productivity will drastically increase. The critical light intensity is approximately 8.9 W·cm^{-2} at the chamber temperature of 50 °C and it decreases to 7.7 W·cm^{-2} at the chamber temperature of 200 °C, which depends on the threshold surface temperature of the Rh/Al nanoantenna

https://doi.org/10.1021/acs.nanolett.1c03215
Nano Lett. 2021, 21, 8824−8830

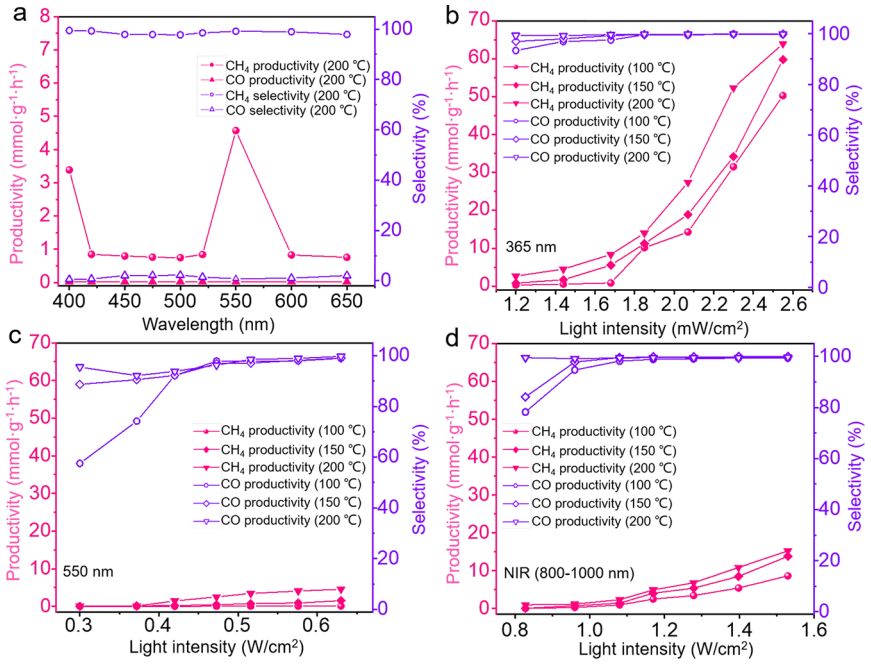

Figure 3. Photothermal CO_2 methanation performance of the Rh/Al nanoantenna catalyst under the light irradiation of various wavelengths and light intensities. (a) CH_4 productivity and selectivity under the irradiation of various monochromatic visible lights (between 400 and 650 nm) at the chamber temperature of 200 °C. CH_4 selectivity and productivity under various intensities of (b) monochromatic UV light (365 nm), (c) monochromatic visible light (550 nm), and (d) NIR light (800−1000 nm) at different chamber temperatures.

catalyst determined by both the chamber temperature and the LSPR-induced surface heating effect.

To further investigate the effect of the chamber temperature on the photothermal CO_2 methanation, the chamber temperature was varied from 50 to 200 °C at a constant light intensity of 11.3 W·cm^{-2} (Figure 2e). When the chamber temperature was increased from 50 to 125 °C, the CH_4 production rate slowly increased from 150 to 200 mmol·g^{-1}·h^{-1}; once the chamber temperature was increased from 150 to 200 °C, the CH_4 production rate sharply increased from 280 to 550 mmol·g^{-1}·h^{-1}, which was a record-breaking CH_4 production rate among the previous reports of solar driven CO_2 methanation.[22] These results indicate that the CH_4 productivity is strongly dependent on the surface temperature of the Rh/Al nanoantenna catalyst. The LSPR-induced heating effect makes the surface temperature of the catalyst greatly exceed the chamber temperature, leading to significantly enhanced CH_4 productivity. This assumption was further confirmed by the CO_2 methanation test at the chamber temperature of 200 °C in the dark (Figure S6). Without incident light, the CH_4 production rate was <1 mmol·g^{-1}·h^{-1} and the CH_4 selectivity decreased to 18%, suggesting that the chamber temperature of 200 °C alone cannot realize high-efficiency CO_2 hydrogenation due to the absence of the LSPR-induced heating effect.

To further clarify the influences of light wavelength and intensity on the performance of Rh/Al nanoantenna catalyst for photothermal CO_2 methanation, we investigated the CH_4 productivity and selectivity under various monochromatic UV and visible lights (365−650 nm) as well as NIR light (800−1000 nm) with the help of different wavelength bandpass filters (Figure 3). The Rh/Al nanoantenna catalyst showed nearly 100% CH_4 selectivity over the whole visible region (Figure 3a), confirming that it could utilize broad-range visible lights to realize highly selective CO_2 methanation. Among these monochromatic visible lights, the irradiation of the 550 nm wavelength allowed the Rh/Al nanoantenna catalyst to achieve the highest CH_4 productivity (4.5 mmol·g^{-1}·h^{-1}).

The synergistic effect of the irradiation wavelength and the chamber temperature was also investigated (Figure 3b−d). The catalytic performance of the Rh/Al nanoantenna catalyst was measured under the irradiation of monochromatic UV light (365 nm), monochromatic visible light (550 nm), and NIR light (800−1000 nm) with various intensities at different chamber temperatures. In Figure 3b, when the intensity of the incident 365 nm UV light was increased from 0.0012 to 0.0026 W·cm^{-2} at the chamber temperature of 100 °C, the CH_4 productivity significantly increased from 0.027 to 50 mmol·g^{-1}·h^{-1}. While under 365 nm UV light irradiation with an intensity of 0.0026 W·cm^{-2}, the CH_4 productivity further increased from 50 to 64 mmol·g^{-1}·h^{-1} as the chamber temperature was raised from 100 to 200 °C. These results confirm that the light intensity and the chamber temperature have a cooperative effect on the reaction rate of CO_2 methanation. Notably, although the power ratio of the 365 nm UV light in the simulated sunlight was very low, the CH_4 productivities measured under the irradiation of the 365 nm UV light (Figure 3b) were much higher than those measured under the monochromatic visible lights at the same conditions (Figure 3a), which shall be ascribed to the stronger LSPR effect induced by the UV light.

For the monochromatic visible light at 550 nm, the cooperative effect of the light intensity and the chamber temperature was also studied (Figure 3c). At a chamber temperature of 100 °C, the CH_4 productivity and selectivity were relatively low under the light intensity of 0.30 W·cm^{-2} (0.005 mmol·g^{-1}·h^{-1} and 57%, respectively) but improved to 0.117 mmol·g^{-1}·h^{-1} and 99% under the light intensity of 0.63 W·cm^{-2}. Meanwhile, with the increase of the light intensity, the yield of the CO byproduct greatly decreased to a very low level. At the chamber temperature of 200 °C, the CH_4

https://doi.org/10.1021/acs.nanolett.1c03215
Nano Lett. 2021, 21, 8824−8830

productivity and selectivity were significantly increased from 0.059 mmol·g^{-1}·h^{-1} and 95% to 4.5 mmol·g^{-1}·h^{-1} and 99%, respectively, when the light intensity increased from 0.30 to 0.63 W·cm^{-2}. It strongly suggested that the incident light intensity and the chamber temperature could cooperate in activating the CO_2 molecule and promoting CH_4 productivity and selectivity. Notably, there was a critical light intensity around 0.37 W·cm^{-2} at the chamber temperature of 200 °C. If the incident light intensity was higher than 0.37 W·cm^{-2}, the CH_4 productivity and selectivity would sharply increase because the surface temperature of the Rh/Al nanoantenna catalyst exceeded the threshold (~450 °C) and greatly promoted CH_4 production.

With the assistance of a NIR bandpass filter, the effects of incident NIR light (800−1000 nm) on the photothermal CO_2 conversion were also investigated (Figure 3d). At the chamber temperature of 100 °C, the CH_4 productivity and selectivity were greatly increased from 0.053 mmol·g^{-1}·h^{-1} and 84% to 7.4 mmol·g^{-1}·h^{-1} and 99%, respectively, when the NIR light intensity was increased from 0.83 to 1.53 W·cm^{-2}, strongly suggesting that the NIR light could also initiate the photothermal effect of the Rh/Al nanostructure. When the chamber temperature was raised to 200 °C, the CH_4 productivity under the NIR light intensity of 1.53 W·cm^{-2} further increased to 13.8 mmol·g^{-1}·h^{-1}. These results confirmed that the Rh/Al nanoantenna catalyst can utilize broad-spectrum lights from the UV region to the NIR region to promote highly efficient CO_2 methanation, and the CH_4 productivity and selectivity can be varied by the incident light intensity, the wavelength, and the chamber temperature, which are the key factors affecting the actual surface temperature of the catalyst. The LSPR-induced photothermal effect and the assistant heating worked together to make the surface temperature of the catalyst exceed the threshold surface temperature, thus promoting the CO_2 methanation reaction. Moreover, Figure S7 indicates the good performance stability of the Rh/Al photothermal catalyst during the long-term catalysis test.

Considering that both Rh and Al could absorb 365 nm UV light, we also investigated the synergetic effect of the Rh and Al nanostructures by comparing the photothermal catalytic performance of the Rh/Al nanoantenna catalyst with a Rh/Al_2O_3 control sample that was prepared using Al_2O_3 instead of Al nanopowder (Figure S8). Under the same light intensity (8.9 or 11.3 W·cm^{-2}), the light absorption capability, surface temperature, and CO_2 methanation performance of Rh/Al_2O_3 were much inferior to those of the Rh/Al sample owing to the absence of the nanoantenna effect.

Generally, CO_2 methanation may follow two different reaction routes according to the absence or presence of *CO intermediates: (1) the association between adsorbed CO_2 and H_2 molecules to form an oxygenate intermediate (*OCHO), followed by subsequent multiple hydrogenation steps to form CH_4; (2) the dissociation of CO_2 to carbonyl $(CO)_{ad}$ and O_{ad}, followed by carbonyl hydrogenation to form CH_4.[23,24] In our case, it is very probable that the photothermal CO_2 methanation of the Rh/Al nanoantenna catalyst took place through the second route (with the presence of *CO intermediates), and the byproduct CO could be further hydrogenated into CH_4 at higher reaction temperatures. To verify this reaction mechanism, an in operando TP-FTIR spectroscopic analysis was conducted to detect the surface species on the Rh/Al nanoantenna catalyst at different surface temperatures (Figure 4). As the surface temperature was increased from 50 to 200 °C, no obvious FTIR signals were

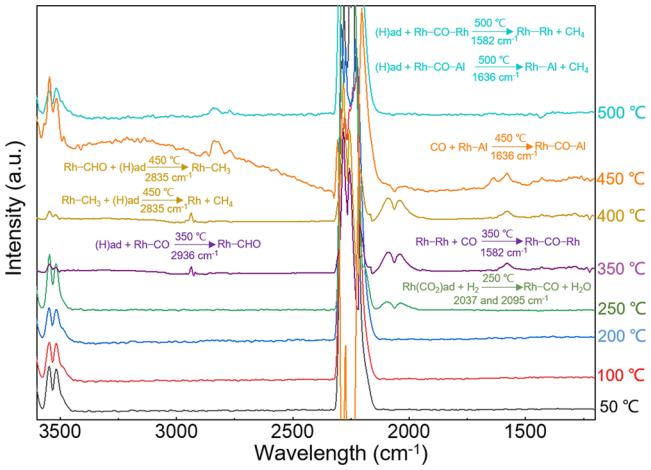

Figure 4. Mechanism studies on the Rh/Al nanoantenna catalyst for CO_2 methanation via in operando TP-FTIR analysis measured at surface temperatures that increased stepwise, indicting the multistep processes for CO_2 activation and conversion.

observed except for the strong characteristic peaks of adsorbed CO_2 molecules between 2150−2350 cm^{-1}. Once the surface temperature was increased to 250 °C, two new peaks emerged at approximately 2095 and 2037 cm^{-1}, corresponding to the symmetrical and antisymmetrical stretching modes of gem-dicarbonyl bonds derived from two linearly or terminally bonded $(CO)_{ad}$ species on a single Rh metal atom, respectively. Moreover, no *CH_x or *OCHO intermediates were detected at the surface temperature of 250 °C. These results proved that $(CO)_{ad}$ species derived from the dissociation of CO_2 molecules was the key intermediate for initiating CO_2 hydrogenation on the Rh/Al nanoantenna catalyst at a relatively low temperature of 250 °C. As the surface temperature was increased to 350 °C, the characteristic peaks of linearly bonded $(CO)_{ad}$ exhibited increased intensities, suggesting the higher surface coverage. Moreover, a new peak appeared at around 1582 cm^{-1}, corresponding to the formation of bridged $(CO)_{ad}$ species between Rh−Rh atoms (Rh−CO−Rh).[25] Moreover, a small peak emerged at approximately 2936 cm^{-1} that was ascribed to Rh−CHO moieties, suggesting that the adsorbed *CO species were hydrogenated to *CHO at 350 °C.[26] At the temperature of 400 °C, the peak intensity of the *CHO species became slightly higher. As the surface temperature was raised to 450 °C, a new peak at approximately 2835 cm^{-1} appeared, which was attributed to the *CH_3 species bonded on the Rh surface.[27] This indicates that the threshold surface temperature for the formation of CH_4 is around 450 °C, and a relatively high surface temperature (≥450 °C) is essential to obtain a high selectivity for the multielectron product CH_4 instead of the two-electron product CO. In addition, a small peak appeared at 1636 cm^{-1}, which could be attributed to the bridge-bonded $(CO)_{ad}$ species between Rh and the Al interface. The hot electrons could be further transferred into the antibonding orbitals of the $(CO)_{ad}$ species for CH_4 production. As the surface temperature was increased to 500 °C, all the peaks related to the $(CO)_{ad}$ species became very weak, suggesting that all the $(CO)_{ad}$ species could be rapidly hydrogenated to CH_4 rather than adsorbed on the catalyst

https://doi.org/10.1021/acs.nanolett.1c03215
Nano Lett. 2021, 21, 8824−8830

surface and leading to a significant increase in the CH_4 productivity. These results confirmed that the CO_2 methanation reaction on the Rh/Al nanoantenna catalyst was a multistep process with CO as a key intermediate as well as a competitive product, especially at temperatures less than 450 °C.

To further verify the important role of CO as the key intermediate for photothermal CO_2 methanation, the reaction behavior was investigated in a $CO/CO_2/H_2$ mixture (1:2.25:6.75 in mole) instead of a CO_2/H_2 mixture (1:3 in mole) (Figure S9). When the incident light intensity was increased from 5.9 to 10.2 $W{\cdot}cm^{-2}$ at a chamber temperature of 50 °C, the CH_4 productivity greatly increased from ∼3 to 230 $mmol{\cdot}g^{-1}{\cdot}h^{-1}$, which is much higher than that in the CO_2/H_2 mixture at the same condition (160 $mmol{\cdot}g^{-1}{\cdot}h^{-1}$, Figure 2c). Meanwhile, the CO conversion ratio increased from 5% to a maximum level of 92%; however, the CO_2 conversion ratio increased from near zero to only ∼7%, suggesting that the CH_4 produced was mainly derived from CO hydrogenation rather than CO_2. As the light intensity was further increased to 11.3 $W{\cdot}cm^{-2}$, the CH_4 productivity reached 237 $mmol{\cdot}g^{-1}{\cdot}h^{-1}$, but the CO conversion ratio slightly decreased to 90%; meanwhile, the CO_2 conversion ratio increased to 15%. This result further verified that the relative high temperature is conducive to CO_2 methanation, which is consistent to the FTIR analysis (Figure 4). CO was preferentially adsorbed and hydrogenated on the surface of the Rh/Al nanoantenna catalyst at relatively low surface temperatures (<450 °C). Once the surface temperature was increased to a higher level (450−700 °C), the CO_2 methanation process was significantly promoted. The above results also proved that the immediate CO could be further hydrogenated into CH_4 with the assistance of the high surface temperature induced by the LSPR effect of Al to overcome the hydrogenation energy barrier to form CH_4.

CONCLUSIONS

In summary, we propose the design of a Rh/Al nanostructure with enhanced LSPR and nanoantenna effects, which exhibits broad-spectrum light absorption over the entire UV−vis-NIR region and a strong photothermal heating effect. Benefitting from the high surface temperature field induced by the photothermal conversion under concentrated simulated sunlight irradiation, the Rh/Al nanoantenna catalyst presented a remarkable catalytic performance for CO_2 methanation, achieving an unprecedented CH_4 production rate of 550 $mol{\cdot}g^{-1}{\cdot}h^{-1}$ and an ultrahigh CH_4 selectivity of nearly 100%. Detailed control experiments and in operando TP-FTIR spectroscopic analysis confirmed that CO_2 methanation on the Rh/Al nanoantenna catalyst was a multistep reaction with CO as a key intermediate as well as a competitive byproduct. We hope this work could bring more insights and inspirations for solar-driven catalysis toward clean and sustainable CO_2-to-fuel conversion.

ASSOCIATED CONTENT

Supporting Information

The Supporting Information is available free of charge at https://pubs.acs.org/doi/10.1021/acs.nanolett.1c03215.

Experimental details; SEM, TEM, and elemental mapping characterizations of the Rh/Al nanoantenna catalyst; apparatus setup for the Co_2 methanation reaction; measurement of the local surface temperature field; ^1H NMR spectrum of the liquid product; CO_2 methanation performance of the catalyst under different conditions; and characterizations and photothermal CO_2 methanation performance of the Rh/Al_2O_3 control sample (PDF)

AUTHOR INFORMATION

Corresponding Author

Zhong Jin − *MOE Key Laboratory of Mesoscopic Chemistry, MOE Key Laboratory of High Performance Polymer Materials and Technology, Jiangsu Key Laboratory of Advanced Organic Materials, School of Chemistry and Chemical Engineering, Nanjing University, Nanjing 210023, China; Shenzhen Research Institute of Nanjing University, Shenzhen 518063, China;* orcid.org/0000-0001-8860-8579; Email: zhongjin@nju.edu.cn

Authors

Gao Fu − *MOE Key Laboratory of Mesoscopic Chemistry, MOE Key Laboratory of High Performance Polymer Materials and Technology, Jiangsu Key Laboratory of Advanced Organic Materials, School of Chemistry and Chemical Engineering, Nanjing University, Nanjing 210023, China; Shenzhen Research Institute of Nanjing University, Shenzhen 518063, China*

Minghang Jiang − *MOE Key Laboratory of Mesoscopic Chemistry, MOE Key Laboratory of High Performance Polymer Materials and Technology, Jiangsu Key Laboratory of Advanced Organic Materials, School of Chemistry and Chemical Engineering, Nanjing University, Nanjing 210023, China; Shenzhen Research Institute of Nanjing University, Shenzhen 518063, China*

Jie Liu − *MOE Key Laboratory of Mesoscopic Chemistry, MOE Key Laboratory of High Performance Polymer Materials and Technology, Jiangsu Key Laboratory of Advanced Organic Materials, School of Chemistry and Chemical Engineering, Nanjing University, Nanjing 210023, China; Shenzhen Research Institute of Nanjing University, Shenzhen 518063, China*

Kaiqiang Zhang − *MOE Key Laboratory of Mesoscopic Chemistry, MOE Key Laboratory of High Performance Polymer Materials and Technology, Jiangsu Key Laboratory of Advanced Organic Materials, School of Chemistry and Chemical Engineering, Nanjing University, Nanjing 210023, China; Shenzhen Research Institute of Nanjing University, Shenzhen 518063, China*

Yi Hu − *MOE Key Laboratory of Mesoscopic Chemistry, MOE Key Laboratory of High Performance Polymer Materials and Technology, Jiangsu Key Laboratory of Advanced Organic Materials, School of Chemistry and Chemical Engineering, Nanjing University, Nanjing 210023, China; Shenzhen Research Institute of Nanjing University, Shenzhen 518063, China*

Yan Xiong − *MOE Key Laboratory of Mesoscopic Chemistry, MOE Key Laboratory of High Performance Polymer Materials and Technology, Jiangsu Key Laboratory of Advanced Organic Materials, School of Chemistry and Chemical Engineering, Nanjing University, Nanjing 210023, China; Shenzhen Research Institute of Nanjing University, Shenzhen 518063, China*

Anyang Tao − *MOE Key Laboratory of Mesoscopic Chemistry, MOE Key Laboratory of High Performance Polymer Materials and Technology, Jiangsu Key Laboratory of*

https://doi.org/10.1021/acs.nanolett.1c03215
Nano Lett. 2021, 21, 8824−8830

Advanced Organic Materials, School of Chemistry and Chemical Engineering, Nanjing University, Nanjing 210023, China; Shenzhen Research Institute of Nanjing University, Shenzhen 518063, China

Zuoxiu Tie − *MOE Key Laboratory of Mesoscopic Chemistry, MOE Key Laboratory of High Performance Polymer Materials and Technology, Jiangsu Key Laboratory of Advanced Organic Materials, School of Chemistry and Chemical Engineering, Nanjing University, Nanjing 210023, China; Shenzhen Research Institute of Nanjing University, Shenzhen 518063, China*

Complete contact information is available at: https://pubs.acs.org/10.1021/acs.nanolett.1c03215

Author Contributions

[‖]These authors contributed equally to this work.

Notes

The authors declare no competing financial interest.

■ ACKNOWLEDGMENTS

This work was supported by the National Key Research and Development Program of China (2017YFA0208200), the Fundamental Research Funds for the Central Universities of China (0205-14380266), the National Natural Science Foundation of China (22022505, 21872069), the Natural Science Foundation of Jiangsu Province (BK20180008), and the Shenzhen Fundamental Research Program of Science, Technology and Innovation Commission of Shenzhen Municipality (JCYJ20180307155007589).

■ REFERENCES

(1) Aziz, M. A. A.; Jalil, A. A.; Triwahyono, S.; Ahmad, A. CO_2 methanation over heterogeneous catalysts: recent progress and future prospects. *Green Chem.* **2015**, *17*, 2647−2663.

(2) Artz, J.; Müller, T. E.; Thenert, K.; Kleinekorte, J.; Meys, R.; Sternberg, A.; Bardow, A.; Leitner, W. Sustainable Conversion of Carbon Dioxide: An Integrated Review of Catalysis and Life Cycle Assessment. *Chem. Rev.* **2018**, *118*, 434−504.

(3) Neatu, S.; Maciá-Agulló, J. A.; Garcia, H. Solar Light Photocatalytic CO_2 Reduction: General Considerations and Selected Bench-Mark Photocatalysts. *Int. J. Mol. Sci.* **2014**, *15*, 5246−5262.

(4) Shehzad, N.; Tahir, M.; Johari, K.; Murugesan, T.; Hussain, M. A critical review on TiO_2 based photocatalytic CO_2 reduction system: Strategies to improve efficiency. *J. CO2 Util.* **2018**, *26*, 98−122.

(5) Nguyen, T. P.; Nguyen, D. L. T.; Nguyen, V.-H.; Le, T.-H.; Vo, D.-V. N.; Trinh, Q. T.; Bae, S.-R.; Chae, S. Y.; Kim, S. Y.; Le, Q. V. Recent Advances in TiO_2-Based Photocatalysts for Reduction of CO_2 to Fuels. *Nanomaterials* **2020**, *10*, 337.

(6) Wang, Y.; Zhao, J.; Li, Y.; Wang, C. Selective photocatalytic CO_2 reduction to CH_4 over Pt/In_2O_3: Significant role of hydrogen adatom. *Appl. Catal., B* **2018**, *226*, 544−553.

(7) Nitopi, S.; Bertheussen, E.; Scott, S. B.; Liu, X.; Engstfeld, A. K.; Horch, S.; Seger, B.; Stephens, I. E. L.; Chan, K.; Hahn, C.; Norskov, J. K.; Jaramillo, T. F.; Chorkendorff, I. Progress and Perspectives of Electrochemical CO_2 Reduction on Copper in Aqueous Electrolyte. *Chem. Rev.* **2019**, *119*, 7610−7672.

(8) Cheng, W. H.; Richter, M. H.; Sullivan, I.; Larson, D. M.; Xiang, C. G.; Brunschwig, B. S.; Atwater, H. A. CO_2 Reduction to CO with 19% Efficiency in a Solar-Driven Gas Diffusion Electrode Flow Cell under Outdoor Solar Illumination. *ACS Energy Lett.* **2020**, *5*, 470−476.

(9) Zhao, H. L.; Zheng, X. Y.; Feng, X. H.; Li, Y. CO_2 Reduction by Plasmonic Au Nanoparticle-Decorated TiO_2 Photocatalyst with an Ultrathin Al_2O_3 Interlayer. *J. Phys. Chem. C* **2018**, *122*, 18949−18956.

(10) Dilla, M.; Pougin, A.; Strunk, J. Evaluation of the plasmonic effect of Au and Ag on Ti-based photocatalysts in the reduction of CO_2 to CH_4. *J. Energy Chem.* **2017**, *26*, 277−283.

(11) Zhang, X.; Li, X. Q.; Zhang, D.; Su, N. Q.; Yang, W. T.; Everitt, H. O.; Liu, J. Product selectivity in plasmonic photocatalysis for carbon dioxide hydrogenation. *Nat. Commun.* **2017**, *8*, 14542.

(12) Zhang, X.; Li, X. Q.; Reish, M. E.; Zhang, Du.; Su, N. Q.; Gutierrez, Y.; Moreno, F.; Yang, W. T.; Everitt, H. O.; Liu, J. Plasmon-Enhanced Catalysis: Distinguishing Thermal and Non-thermal Effects. *Nano Lett.* **2018**, *18*, 1714−1723.

(13) Zhou, L. N.; Swearer, D. F.; Zhang, C.; Robatjazi, H.; Zhao, H. Q.; Henderson, L.; Dong, L. L.; Christopher, P.; Carter, E. A.; Nordlander, P.; Halas, N. J. Quantifying hot carrier and thermal contributions in plasmonic photocatalysis. *Science* **2018**, *362*, 69−72.

(14) Aslam, U.; Rao, V. G.; Chavez, S.; Linic, S. Catalytic conversion o solar to chemical energy on plasmonic metal nanostructures. *Nat. Catal.* **2018**, *1*, 656−665.

(15) Swearer, D. F.; Leary, R. K.; Newell, R.; Yazdi, S.; Robatjazi, H.; Zhang, Y.; Renard, D.; Nordlander, P.; Midgley, P. A.; Halas, N. J.; Ringe, E. Transition-Metal Decorated Aluminum Nanocrystals. *ACS Nano* **2017**, *11*, 10281−10288.

(16) Ulmer, U.; Dingle, T.; Duchesne, P. N.; Morris, R. H.; Tavasoli, A.; Wood, T.; Ozin, G. A. Fundamentals and applications of photocatalytic CO_2 methanation. *Nat. Commun.* **2019**, *10*, 3169.

(17) Su, M. N.; Dongare, P. D.; Chakraborty, D.; Zhang, Y.; Yi, C.; Wen, F.; Chang, W. S.; Nordlander, P.; Sader, J. E.; Halas, N. J.; Link, S. Optomechanics of Single Aluminum Nanodisks. *Nano Lett.* **2017**, *17*, 2575−2583.

(18) Robatjazi, H.; Zhao, H.; Swearer, D. F.; Hogan, N. J.; Zhou, L.; Alabastri, A.; McClain, M. J.; Nordlander, P.; Halas, N. J. Plasmon-induced selective carbon dioxide conversion on earth-abundant aluminum-cuprous oxide antenna-reactor nanoparticles. *Nat. Commun.* **2017**, *8*, 27.

(19) Sarathi, R.; Sindhu, T. K.; Chakravarthy, S. R. Generation of nano aluminium powder through wire explosion process and its characterization. *Mater. Charact.* **2007**, *58*, 148−155.

(20) Lerner, M. I.; Glazkova, E. A.; Lozhkomoev, A. S.; Svarovskaya, N. V.; Bakina, O. V.; Pervikov, A. V.; Psakhie, S. G. Synthesis of Al nanoparticles and Al/AlN composite nanoparticles by electrical explosion of aluminum wires in argon and nitrogen. *Powder Technol.* **2016**, *295*, 307−314.

(21) Larichev, Y. V.; Netskina, O. V.; Komova, O. V.; Simagina, V. I. Comparative XPS study of Rh/Al_2O_3 and Rh/TiO_2 as catalysts for $NaBH_4$ hydrolysis. *Int. J. Hydrogen Energy* **2010**, *35*, 6501−6507.

(22) He, J.; Janáky, C. Recent Advances in Solar-Driven Carbon Dioxide Conversion: Expectations versus Reality. *ACS Energy Lett.* **2020**, *5*, 1996−2004.

(23) Aziz, M. A. A.; Jalil, A. A.; Triwahyono, S.; Ahmad, A. CO_2 methanation over heterogeneous catalysts: recent progress and future prospects. *Green Chem.* **2015**, *17*, 2647−2663.

(24) Jenewein, B.; Fuchs, M.; Hayek, K. The CO methanation on Rh/CeO_2 and CeO_2/Rh model catalysts: a comparative study. *Surf. Sci.* **2003**, *532*−*535*, 364−369.

(25) Miao, B.; Ma, S. S. K.; Wang, X.; Su, H.; Chan, S. H. Catalysis mechanisms of CO_2 and CO methanation. *Catal. Sci. Technol.* **2016**, *6*, 4048−4058.

(26) Li, W.; Wang, H.; Jiang, X.; Zhu, J.; Liu, Z.; Guo, X.; Song, C. A short review of recent advances in CO_2 hydrogenation to hydrocarbons over heterogeneous catalysts. *RSC Adv.* **2018**, *8*, 7651−7669.

(27) Martin, N. M.; Hemmingsson, F.; Schaefer, A.; Ek, M.; Merte, L. R.; Hejral, U.; Gustafson, J.; Skoglundh, M.; Dippel, A. C.; Gutowski, O.; Bauer, M.; Carlsson, P. A. Structure−function relationship for CO_2 methanation over ceria supported Rh and Ni catalysts under atmospheric pressure conditions. *Catal. Sci. Technol.* **2019**, *9*, 1644−1653.